Electronic structure of $Sn_2P_2S_6$

K. Kuepper,* B. Schneider, V. Caciuc,† and M. Neumann
University of Osnabrueck, Department of Physics, Barbarastrasse 7, D-49069 Osnabrueck, Germany

A. V. Postnikov
Institute of Metal Physics, S. Kowalewskoj 18, 620219 Yekaterinburg, Russia

A. Ruediger
University of Cambridge, Department of Earth Sciences, Downing Street, Cambridge CB2 3EQ, United Kingdom

A. A. Grabar and Yu. M. Vysochanskii
Uzhgorod University, Pidhirna 46, 88000 Uzhgorod, Ukraine

(Received 2 August 2002; revised manuscript received 24 November 2002; published 3 March 2003)

The electronic properties of the ferroelectric compound $Sn_2P_2S_6$ are investigated by x-ray photoelectron spectroscopy and soft x-ray fluorescence spectroscopy. Excellent agreement between theoretical calculations and experimental data for the electronic structure of the investigated compound is achieved. With help of the Sn core level spectra it is confirmed that the compound contains Sn^{2+} ions. The valence band mainly consists of five resolvable bands between 3.3 eV and 14.5 eV. Consistent with the results of band-structure calculation and the soft x-ray fluorescence spectra, $Sn_2P_2S_6$ can be viewed as an ionic crystal, built of Sn^{2+} and the $(P_2S_6)^{4-}$ fragments. Within the latter, P-P and P-S bonds are largely covalent and characterized by sp hybridization.

DOI: 10.1103/PhysRevB.67.115101 PACS number(s): 71.20.−b, 77.84.−s, 78.70.En, 79.60.−i

I. INTRODUCTION

The best known inorganic photorefractive crystals are ferroelctric oxides, such as $LiNbO_3$ or $Ba_{0.77}Ca_{0.23}TiO_3$.[1] Nonoxidic tin hypothiodiphosphate ($Sn_2P_2S_6$) is however also a ferroelectric with remarkable photorefractive properties.[2–4] Special emphasis was given to its fast holographic response at 1064 nm for optical applications; fast holography by band-band transition has also been realized.[5]

In contrast to most industrially relevant ferroelectrics, which are insulators, $Sn_2P_2S_6$, due to its small band gap of 2.3 eV at room temperature, has pronounced semiconductor features. Band-band excitation results in persistent conductivity,[6] usually discussed in terms of a large lattice relaxation resulting in a strong Stokes shift.[7]

The compound of our interest belongs to a broad family with the generic formula $MM'P_2X_6$ (M, M'=Sn, Cu, In, Pb, Fe, Mn, Cr, . . . ;X=S, Se), which crystallize in three-dimensional or layered crystal structures and illustrate different types of dipole ordering—ferroelectric, ferrielectric, or incommensurate modulation of a spontaneous polarization.[8–11] Obviously mobile ethanelike P_2X_6 groups permit to arrange different morphologies of the crystal structure and different cooperative dipole behavior at different metal cations. For the layered crystals $CuInP_2(S/Se)_6$, the appearance of ferrielectric phases was analyzed as a result of strong interplay between electronic and crystallographic instabilities by the *s* second order Jahn-Teller effect related to the d^{10} electronic configuration of the Cu cations.[12] In the case of $Sn_2P_2(S/Se)_6$ crystals with three-dimensional crystal structures, a driving force for a ferroelectric phase appearance is supposed to be mainly attributed to a lone free-electron pair of the Sn cations.[13] In a composition-temperature phase diagram of the crystal solid solutions for $Sn_2P_2(Se_xS_{1-x})_6$, the Lifshitz point, where the paraelectric, ferroelectric, and incommensurate phases meet, is at $x=0.28$.[8] There is also a virtual tricritical point, which together with long-range dipole interaction determines specific critical behavior of thermodynamic properties in a region of the phase transitions.[14–17] According to experimental evidence, ferroelectric phase transitions in $Sn_21P_2X_6$ (X=S, Se) indicate a crossover between the order-disorder and displacive type. The softening of an optical mode was observed in Raman-scattering[18] and neutron scattering[19,20] spectra. Very recently, a complete spectrum of long-wavelength phonon modes in $Sn_2P_2S_6$ by Raman scattering has been published.[21]

The crystal structure of $Sn_2P_2S_6$ has been refined in a sequence of measurements.[22–25] The room-temperature phase is a (ferroelectric) monoclinic one, with the space group Pn (No. 7). Above about 66 °C the crystal undergoes a transition into another monoclinic phase, possessing the center of inversion (space group $P2_1/c$, No. 14). The phase transition was argued to be of the second order,[25] with ''off-center'' Sn displacement playing the role of the order parameter. The ferroelectric phase is referred to in the literature as monoclinic (II).[22,23] Microscopically, the structure is characterized by PS_3-PS_3 units (with P-P and P-S distances of 2.2 and 2.0 Å, respectively[25]), which are held together by S-Sn interactions. The immediate neighborhood of Sn atoms is therefore the shell of eight S atoms, roughly arranged as a bicapped trigonal prism. At elevated temperatures (e.g., 110 °C, as measured in Ref. 25), the Sn-S distances vary between 2.91 and 3.23 Å, maintaining the inversion symmetry around a midpoint between two Sn atoms. In the room-temperature (ferroelectric) phase, this inversion symmetry is broken, as

the range of Sn-S distances becomes 2.78–3.46 Å around one Sn atom and 2.88–3.52 Å around the other one.[25] That means that the Sn atoms become crystallographically nonequivalent and displace inside their respective (almost rigid) S_8 cages differently. One even discusses this in terms of reduced (8 to 7) coordination of half of the Sn atoms in the ferroelectric phase. Indeed, one was able to observe different hole-binding properties for such unequivalent Sn ions.[26]

However, for the analysis of spatial distribution of the electron density and chemical bonding (that is essential for both ferroelectric instability and optical characteristics), the methods of x-ray and photoelectron spectroscopy provide a tool of unique precision, especially useful in combination with first-principle electronic structure studies. Due to a relative complexity and low symmetry of crystals, such studies long remained unfeasible even for compositionally homogeneous systems. Recently, however, a profound electronic structure analysis appeared for $Sn_2P_2Se_6$, based on plane-wave calculations.[27] Moreover, for $CuInP_2Se_6$ a band-structure calculation by the linear muffin-tin orbitals method has been presented, in combination with an ultraviolet photoemission study.[12] We failed to find any earlier first-principles calculations for $Sn_2P_2S_6$, apart from preliminary reports by Fenchak *et al.*,[28] which, however, restricted to just 1 f.u. per primitive cell and thus neglected the glide plane symmetry of the crystal. Although there are some photoemission measurements confirming the existence of Sn^{2+} ions,[29] as well as some x-ray fluorescence and absorption spectra have been reported,[30,31] we present here a more complete systematic study of superior quality. Specifically, the experimental side is x-ray photoelectron spectroscopy (XPS) and soft x-ray fluorescence (SXF) spectroscopy. The band-structure calculations are performed with the full-potential linearized augmented plane-wave (FLAPW) method.[32]

II. EXPERIMENTAL AND THEORETICAL DETAILS

All spectra are recorded at room temperature, the crystals were in the ferroelectric monoclinic (II) phase. For all measurements, small single crystals are available, produced by a gas transport reaction method in evacuated quartz ampoules with I_2 as the transporter.

XPS spectra are recorded using a PHI 5600ci multitechnique spectrometer with monochromatic Al $K\alpha$ ($h\nu = 1486.6$ eV) radiation of 0.3 eV full width at half maximum. The resolution of the analyzer is 1.5% of the pass energy, i.e., 0.45 eV. All spectra are obtained using 400-μm-diameter analysis area. During the measurements, the pressure in the main chamber is kept below 3×10^{-9} mbars. The single crystals are cleaved *in situ*. The survey spectrum taken directly after breaking the samples shows no contamination of oxygen but a rather low one of the hydrocarbon, C $2p$ states that should have no influence on the valence-band spectra. Because of the samples being insulators or large band-gap semiconductors, a charging effect is observed. All spectra are corrected for this charging effect using the carbon $1s$ line of adsorbed carbon ($E_B = 285.0$ eV).[33]

Soft x-ray fluorescence measurements are performed at the beam line 8.0.1 of the Advanced Light Source at Lawrence Berkeley Laboratory. The undulator beamline is equipped with a spherical grating monochromator.[34] Fluorescent radiation emitted by the sample was analyzed using a high-resolution grating spectrometer and a multichannel detector.

TABLE I. Stoichiometry of $Sn_2P_2S_6$.

Core level	AC (experimental) (%)	AC (optimum) (%)
Sn $3d_{5/2}$	19	20
P $2p$	21	20
S $2p$	60	60

As regards the calculation, even as we are not concentrating on total-energy issues in the present study, the fact that the compound in question is loosely packed, with a strongly varying electron density in large interatomic regions, demands for the use of a full-potential electronic calculation scheme. We use the linearized augmented plane-wave method as implemented in the WIEN97 code.[32] The exchange-correlation energy functional is treated in the local-density approximation (LDA) as parametrized by Perdew and Wang.[35] To relax the linearization errors, the Sn $4p$ and $4d$, P $3s$, and S $3s$ semicore states are treated with the introduction of local orbitals in the basis set.[36] Brillouin-zone integrations are performed using the improved tetrahedron method[37] on a $4\times4\times4$ special k-point mesh, which generates 21 k points in the irreducible Brillouin zone. We use muffin-tin radii of 2.2 a.u. for Sn, 1.9 a.u. for P and S. With this option, the plane-wave cutoff parameter $R_{\min}K_{\max}$, which controls the size of the basis, is set to 7.0 and results in, on the average, 2606 basis functions for each k point. The use of a denser k mesh as well as a higher cutoff parameter reveals no significant influence on the results presented in this paper. Moreover, these calculations are being done using the experimental lattice parameters.[24]

III. RESULTS AND DISCUSSION

A. Core levels

First we want to discuss the chemical environment of the different chemical elements and the atomic concentration on the basis of the core-level spectra. The most intense lines are selected to specify the stoichiometry of the compound. After subtraction of a Tougaard-type inelastic background[38] and taking into account the photoelectron cross sections, the atomic concentration can be specified by the peak areas. The results are listed in Table I.

The experimentally determined atomic concentration is in good agreement with the ideal stoichiometry of the compound. As one result, we can summarize that the crystals have a high quality with regard to the chemical purity. However, it is known that, e.g., in the oxides mentioned above, oxygen vacancies in much lower concentrations than detectable with the present setup contribute significantly to the defect structure and thus to the light induced charge transfer in these materials. It has been also shown that a deficiency of sulfur in $Sn_2P_2S_6$ leads to high values of the conductivity.[39]

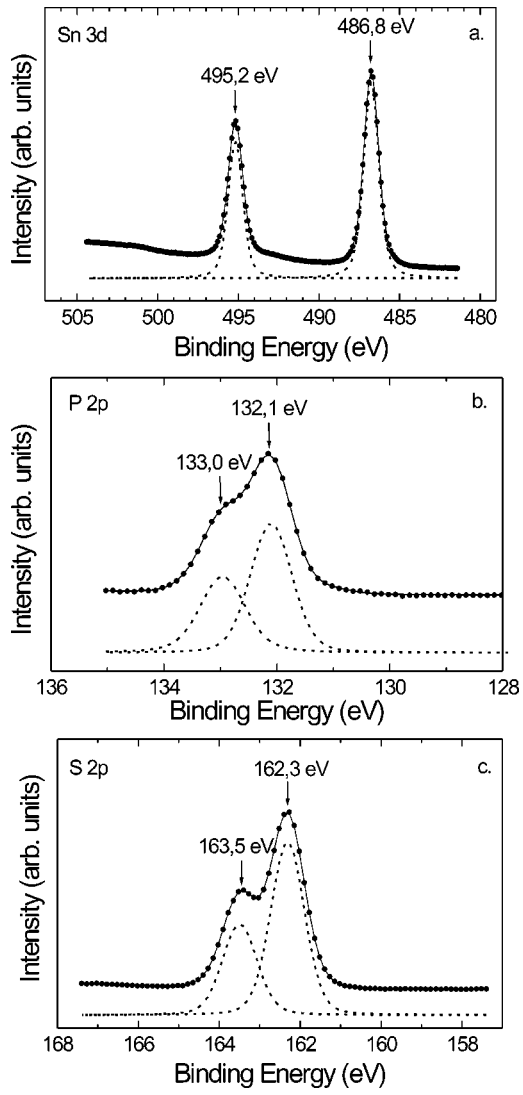

FIG. 1. XPS spectra of the Sn $3d$ (a), P $2p$ (b), and S $2p$ (c) core levels. Experimental data are presented in full circles; best fit is indicated by the thin black line. The dashed lines show fitted Gaussian-Lorentzian curves.

In Fig. 1 we present the x-ray photoemission data that were recorded of the most intensive core levels of $Sn_2P_2S_6$. The Sn $3d$ states $j=5/2$ and $j=3/2$ are clearly resolved with a spin-orbit splitting of 8.6 eV. The Sn $3d_{5/2}$ state is located at a binding energy (E_B) of 486.8 eV. Compared to the reference of metallic tin ($E_B=485.0$ eV) this is an increase of 1.8 eV, which is in good agreement with measurements on SnO (Ref. 33) and results from Currò *et al.*[29] We confirm that tin in $Sn_2P_2S_6$ occurs as Sn^{2+} ions. The data that the Sn ion is in the $2+$ state with very high ionicity (≈ 1.6) was also obtained independently by Mössbauer spectroscopy.[40]

Figures 1(b) and 1(c) show the data of the P $2p$ and S $2p$ core levels. The S $2p$ core level can be clearly resolved with a spin-orbit splitting of 1.2 eV. P $2p_{1/2}$ core levels are still detectable as a shoulder with a spin-orbit splitting of 0.9 eV. The binding energy for the P $2p_{3/2}$ core-level state of elemental P is 130.0 eV,[33] and for S $2p_{3/2}$ core level states of elemental S is 164 eV.[33] So the P $2p$ level in $Sn_2P_2S_6$ has shifted by 2.1 eV to higher binding energies, the S $2p$ level by 1.7 eV to lower binding energies. This indicates that sulfur in $Sn_2P_2S_6$ is charged negatively, while phosphorus is charged positively. Further discussion will be realized on the basis of the valence-band measurement, the SXF spectra, and the band-structure calculations.

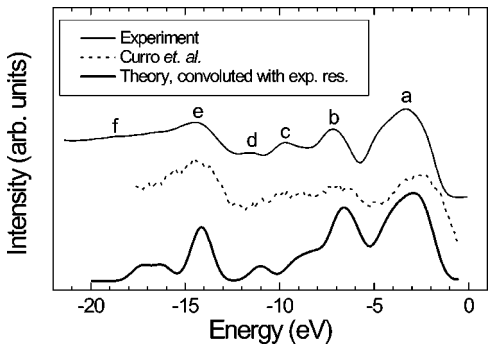

FIG. 2. X-ray photoelectron valence-band spectra of $Sn_2P_2S_6$. Solid line: measured valence spectrum. Dashed line: spectrum quoted from Currò *et al.* (Ref. 29) for comparison. Below: Result of the FLAPW calculation, convoluted with our experimental resolution.

B. Valence band and SXF spectra

X-ray photoelectron spectroscopy of the valence band provides data of the occupied total density of states. In Fig. 2 we illustrate the valence-band x-ray photoelectron spectra of $Sn_2P_2S_6$. To compare the experimental data with theoretical results, in the following binding energies are reversed.

According to the results, this compound contains Sn^{2+} ions, i.e., Sn has lost its $5p$ electrons. The valence band is therefore dominated by Sn $5s$, S $3s$, S $3p$, P $3s$, and P $3p$ levels. Our measurements of the valence-band spectrum indicate five distinguishable bands at -3.3 eV, -7.2 eV, -9.7 eV, -11.5 eV, and -14.5 eV, labeled a–e, in contrast with the measurements of Currò *et al.*,[29] which only resolved three regions. A peak near the Fermi level and a peak located at -14.5 eV are in good agreement with our measurement (states labeled *a* and *e*). The bands *b*, *c*, and *d* differ from the results of Currò *et al.*[29] For bands denoted *a*, *b*, and *d* excellent agreement between experiment and theory for the position is achieved. The calculation indicates band *c* as a shoulder of band *b*; in comparison with the experimental data, band *c* also shows a shift of 1 eV. For bands *e* and *f*, the calculations predict higher intensities than measured.

The results of our FLAPW band-structure calculations and the measured valence-band structure are shown in Fig. 3. The calculation provides results for the total density of states (TDOS) and the partial density of states (PDOS) of all three constituents.

The density of states (Fig. 3), due to its decomposition into *l*-resolved contributions in the muffin-tin spheres (Fig. 4), can be understood as follows.[41]

All three constituents show clear separation of their corresponding *s* and *p* states, on which the effects of hybridization are imposed. For Sn, the separation between $5s$ and $5p$

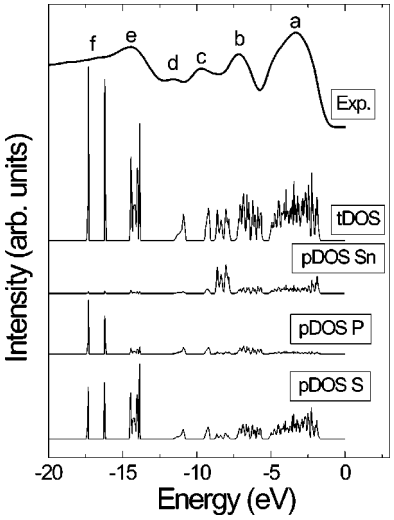

FIG. 3. X-ray photoelectron valence-band spectrum of $Sn_2P_2S_6$ and results of the band-structure calculation; total (TDOS) and partial (PDOS, for three constituents) densities of states.

''centers of gravity'' is about 10 eV, whereby Sn 5*p* lies clearly above the Fermi level (but for a small admixture to the S 3*p* states), thus supporting the above-mentioned experimental conclusion of essential ionization to the Sn^{2+} state. The electron density from Sn goes primarily to the neighboring S atoms, yielding almost full occupation of the S 3*p* band. The S 3*s*-3*p* separation is, according to the calculation, about 12 eV, with quite a narrow S 3*s* band. A low dispersion of the latter is a consequence of structure arrangement, where S atoms are far apart, connected either via common Sn neighbors (that have, however, no electronic states of their own in the energy region of S 3*s*), or through the P-P bridges. The phosphorus atoms are covalent glue in the structure. Not much electronegative themselves, and out of direct contact with Sn^{2+} ions, they have, according to their nominal position in the periodic table, a half-filled 3*p* shell, due to a huge splitting of the latter into bonding and antibonding parts. A direct P-P covalent bonding also splits the P 3*s* states, otherwise well localized and deeper than S 3*s* by about 1.5 eV into bonding (lower) and antibonding (upper) states. Furthermore, the interaction of S 3*s* with such P-P hybridized states produces a replica of this doublet near -10 eV. Whereas the lowest pair of states is P-S bonding, the higher-energy replica is P-S antibonding. The latter P-S antibonding doublet appears (with different weights) in both S 3*s* and P 3*s* partial densities of states. Similar separated groups of bands have been found by Caracas and Gonze[27] in their calculation for the isoelectronic compound $Sn_2P_2Se_6$.

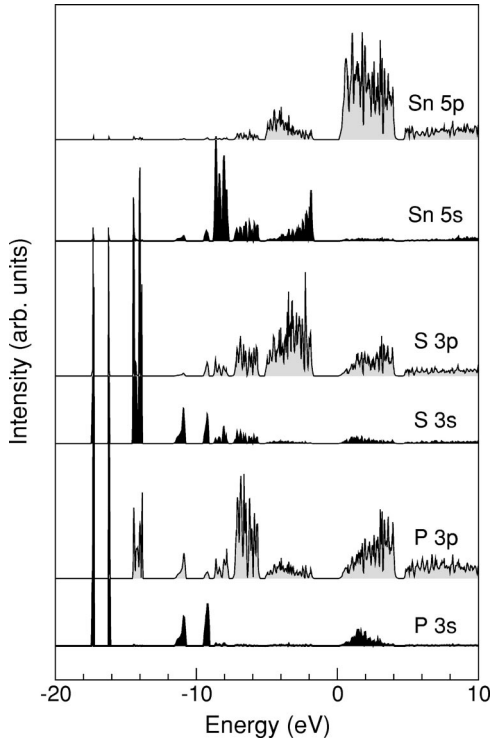

FIG. 4. The calculated partial density of states of Sn and P, split into *s* states and *p* states.

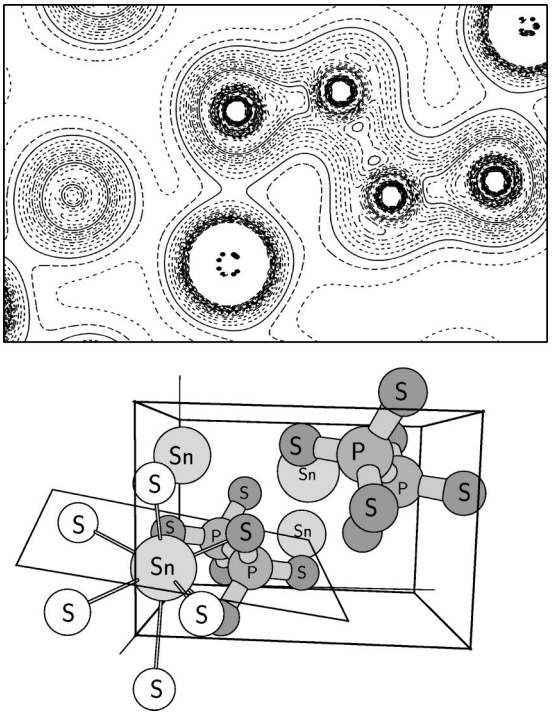

FIG. 5. Top panel: contour plot of the charge density in the plane indicated in the lower panel. The plane passes through Sn, S, and P atoms (in the middle of the plot) and is almost coplanar with the S-P-P-S zigzag (that is a cut through the P_2S_6 cluster). Other S atoms (left middle and top left) are slightly out of the plane. The plot area is 10.39×6.35 Å^2. The countour planes are equidistant at $0.075e/$Å^3. Bottom panel: Unit cell of $Sn_2P_2S_6$ with 2 f.u. (shown in gray) and some additional S atoms (in white) obtained by translation to complete the near-neighbor shell of a Sn atom.

These considerations from the analysis of PDOS can be further illustrated by the spatial distribution of the electron density. In Fig. 5 the cut is done through three consecutive Sn-S-P atoms, and their other neighbors almost in, or slightly off, this plane. One sees a striking contrast between an ionized shape of Sn atoms (indicated by perfect sphericity of the electron density in its neighborhood) and a strong covalency

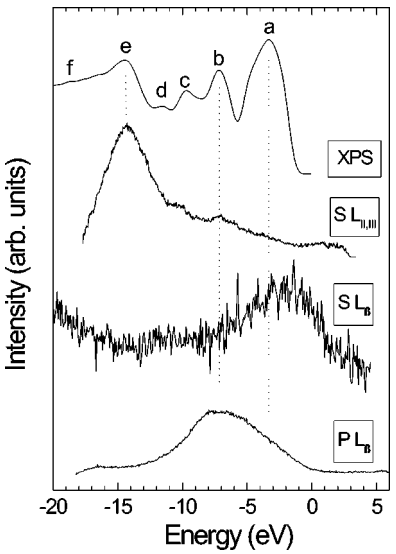

FIG. 6. Comparison of the XPS valence-band spectrum of $Sn_2P_2S_6$ with the S $L_{II,III}$, S L_β, and the P L_β SXF spectra.

along the S-P-P-S chains. The latter exhibits a charge-density distribution resembling that in tetragonally directioned Si stuctures. One notices, moreover, an electron-density displacement from phosphorus to sulfur atoms. Away from P_2S_6 groups and Sn ions docked between them, there is hardly any charge density accumulated. Again, very similar charge-density plots were found in Ref. 27 for $Sn_2P_2Se_6$ (with the difference that pseudopotentials have been used in the latter case so that intra-atomic structure is missing).

An experimental support for the identification of features in the XPS comes from soft x-ray fluorescence measurements. Figure 6 compares the XPS valence-band results with the S $L_{II,III}$, S L_β, and P L_β SXF spectra. SXF spectra are converted with the XPS binding energies to the binding-energy scale. The S $L_{II,III}$ spectrum is due to the S $3s \rightarrow 2p$ transition and dominated by a peak at -15 eV. Two additional features in the S $L_{II,III}$ spectrum can be seen at -10 and -7 eV. The P_β SXF spectrum (P $3p \rightarrow 2s$ transition) is a single strongly broadened peak, roughly revealing the bulk of the P $3p$ states, with a maximum around -7 eV. The S L_β emission spectrum (S $3p \rightarrow 2s$ transition) is of inferior intensity but allows nevertheless to identify the maximum at ~ -3 to -1 eV. Tin contributes no SXF spectra, since it is impossible to achieve any excitation out of the $5p$ and the $5s$ states into the $3d$ state and no fluorescence can be investigated. This is explained by the XPS measurements that indicate a complete ionization of tin in $Sn_2P_2S_6$. Also the obtained fluorescense out of the $5s$ into the $3p$ state is very weak due to a low probability for this transition.

C. Discussion

The analysis of the x-ray emission data along with XPS and the calculation results yields the following. The S L_β emission spectrum (maximum at ~ -3 to -1 eV) is due to the S $3p$ states as is clearly seen from the corresponding PDOS. These states are the principal contributors to the feature *a* in the XPS. In the absence of Sn emission spectra, we proceed with the attribution of features due to Sn in the XPS based on the calculation results only. The Sn $5s$ and in part also the $5p$ states hybridize with S $3p$ and hence yield a contribution to the feature *a*. Feature *b* in the XPS is mainly attributed to the (occupied part of) P $3p$ states, as the P_β SXF spectrum (maximum around -7 eV), roughly revealing the bulk of the P $3p$ states, confirms. P $3p$ states hybridize with S $3s$ corresponding to the feature at -7 eV in the S $L_{II,III}$ emission spectrum. The calculated PDOS confirms hybridization effects of P $3p$ states not only with S $3s$ states, but also predicts P $3p$ states hybridizing with S $3p$ states. The ''generic'' position of the Sn $5s$ states, not affected by the hybridization with sulfur, is near -9 eV. The corresponding pronounced peak in the calculated Sn $5s$ PDOS seems to contribute to the feature *c* in the XPS. The feature at -10 eV in the S $L_{II,III}$ reveals hybridization effects of S $3s$ with P $3s$ and P $3p$ states. The peaks at these positions are clearly seen in the calculated PDOS; that around -10 eV is actually split by ~ 1.5 eV and emerges in the XPS as features *d*,*c*, not resolved in the S $L_{II,III}$ emission spectrum. The S $L_{II,III}$ spectrum shows a maximum peak revealing the position of S $3s$ states, at -15 eV. This is consistent with the calculated result and hence unambiguously attributes the feature *e* in the XPS. Finally, the feature *f* in the XPS manifests the P $3s$ states.

To conclude the comparison of XES (PDOS) with the XPS (TDOS), one can discuss the position of *s* levels of three constituents. It is known for oxides that the position of the O $2s$ band in the LDA may be off by as much as 2.5 eV (O $2s$ binding energy underestimated in the calculation), because the core hole relaxation in a relatively localized O $2s$ shell adds to the binding energy. This aspect is neglected in a conventional LDA calculation but accessible in a quasiparticle band-structure treatment. One would expect this effect to be less pronounced in sulphides, due to anticipated weaker localization of the S $3s$ states. Indeed, we note a good agreement in the position of the S $3s$ peak in the DOS with the feature *e* in the XPS. For Sn, where the shallow $5s$ state is essentially ''bandlike,'' the agreement in the energy position is also good (although the corresponding feature *c* in the XPS is rather weak). On the contrary, for phosphorus with its deeper and quite localized $3s$ states, one would expect a discrepancy between the LDA calculation and the XPS of the order of that in oxides. The corresponding feature *f* is, however, too weak in the XPS to address this issue in more detail. Other electronic bands in the compound in question do not seem to demand for a special treatment of correlation effects beyond the LDA for understanding the spectroscopy of this material in a satisfactory way.

In combination with the x-ray photoelectron measurements and the results of the band-structure calculation, we get the following interpretation of the electronic structure of $Sn_2P_2S_6$. Sulfur and phosphorus can be treated as a $(P_2S_6)^{4-}$ cluster with a strong internal covalent bonding between P and S. Sulfur has a higher electron affinity compared to phosphorus and, therefore, is negatively charged confirmed by the chemical shift of the S $2p$ x-ray photoemission spectrum to lower binding energies. A SXF measurement of

TABLE II. The result of the XPS measurement of the valence band of $Sn_2P_2S_6$, including the discussed assignment of the particular bands.

Band	Energy position (XPS) (eV)	Assignment
a	−3.3	S 3*p*/P 3*p*
b	−7.2	P 3*p*/S 3*s*
c	−9.7	P 3*s*/Sn 5*s*
d	−11.5	S 3*s*/P 3*s*
e	−14.5	S 3*s*

the P $3s \rightarrow$ P $2p$ transition (P $L_{\mathrm{II,III}}$) is not yet available. With such a spectrum, it could be clarified whether the bands *c* and *f* are formed by P 3*s*, as the calculation predicts. According to bands *e* and *f*, the calculation predicts a higher intensity than observed by XPS. This is due to the lack of sensitivity factors in our band-structure calculation. The sensitivity factors include among other things photoelectric cross sections for the atomic orbital of interest and a geometric efficiency factor for the instrumental arrangement. Table II summarizes the results of this spectroscopic study of the valence band of $Sn_2P_2S_6$.

IV. CONCLUSIONS

As a result of this combined study of the electronic band structure of tin hypothiodiphosphate ($Sn_2P_2S_6$) using XPS and SXF measurements and theoretical FLAPW band-structure calculations, we can assign the measured XPS data to the electronic states in the valence band of $Sn_2P_2S_6$. The bonding between both of the unequal Sn^{2+} ions and the $(P_2S_6)^{4-}$ cluster is ionic, inside the cluster we have evidence of strong covalent bonding between phosphorus and sulfur. We observe *sp* hybridization between P and S, dominating the center of the valence band, where some influence of Sn 5*s* states is also present. The results by means of XPS and SXF represent the experimental background for *ab initio* modeling, including defect and impurity states. Due to a good agreement between experimental spectra and first-principles calculations, an unambiguous identification of all spectral features became possible. This provides a basis for future studies and understanding the electronic structure of related mixed compounds.

ACKNOWLEDGMENTS

This work was supported by the Deutsche Forschungsgemeinschaft (DFG), SFB 225. Financial support by the Ph.D. program of Lower Saxony is gratefully acknowledged. The authors are grateful to G. Borstel for mediating the access to computer facilities. We want to thank O. F. Schirmer for continous serious discussions. We are grateful to S. G. Odoulov for helpful support. One of us, A.R., would like to thank the Alexander von Humboldt Foundation for generous support.

*Electronic address: kkuepper@uos.de
†Present address: Institut für Festkörperforschung, Forschungszentrum Jülich, D-52425 Jülich, Germany.

[1] K. Buse, Appl. Phys. B: Lasers Opt. **64**, 391 (1997).
[2] S.G. Odoulov, A.N. Shumelyuk, U. Hellwig, R.R. Rupp, A.A. Grabar, and I.M. Stoyka, J. Opt. Soc. Am. B **13**, 2352 (1996).
[3] A.A. Grabar, I.V. Kedyk, M.I. Gurzan, I.M. Stoyka, A.A. Molnar, and Y.M. Vysochanskii, Opt. Commun. **188**, 187 (2001).
[4] A. Shumelyuk, S.G. Odoulov, D. Kip, and E. Krätzig, Appl. Phys. B: Lasers Opt. **72**, 707 (2001).
[5] R. Ryf, G. Montemezzani, P. Günter, A.A. Grabar, and I.M. Stoyka, OSA Trends Opt. Photonics Ser. **27**, 80 (1999).
[6] A. Grabar, Ferroelectrics **192**, 155 (1997).
[7] G. Watkins, Mater. Sci. Forum **38**, 39 (1989).
[8] Y. Vysochanskii and V. Slivka, Sov. Phys. Usp. **35**, 123 (1992).
[9] V. Maisonneuve, V. Cajipe, A. Simon, R.V.D. Muhll, and J. Ravez, Phys. Rev. B **56**, 10 860 (1997).
[10] Y. Vysochanskii, V. Stephanovich, A. Molnar, V. Cajipe, and X. Bourdon, Phys. Rev. B **58**, 9119 (1998).
[11] Y. Vysochanskii, A. Molnar, M. Gurzanand, V. Cajipe, and X. Bourdon, Solid State Commun. **115**, 13 (2000).
[12] Y. Fagot-Revurat, X. Bourdon, F. Bertran, V. Cajipe, and D. Malterre (unpublished).
[13] R. Enjalbert, J. Galy, Y. Vysochanskii, A. Ouedraogo, and P. Saint-Gregoire, Eur. Phys. J. B **8**, 169 (1999).
[14] Y. Vysochanskii, M. Major, V. Rizak, V. Slivka, and M. Khoma, Sov. Phys. JETP **68**, 782 (1989).
[15] Y. Sereda, Phys. Rev. B **66**, 054109 (2002).
[16] R. Folk and G. Moser, Phys. Rev. B **47**, 13 992 (1993).
[17] R. Folk, Phase Transitions **67**, 645 (1999).
[18] P.V. Loosdrecht *et al.*, Phys. Rev. B **48**, 6014 (1993).
[19] S. Eijt, R. Currat, J. Lorentzo, P. Saint-Gregoire, B. Hennion, and Y. Vysochanskii, Eur. Phys. J. B **5**, 169 (1998).
[20] S. Eijt, R. Currat, J. Lorentzo, P. Saint-Gregoire, S. Katano, T. Janssen, B. Hennion, and Y. Vysochanskii, J. Phys.: Condens. Matter **10**, 4811 (1998).
[21] J. Hlinka, I. Gregora, and V. Vorlicek, Phys. Rev. B **65**, 064308 (2002).
[22] W. Klingen, R. Ott, and H. Hahn, Z. Anorg. Allg. Chem. **369**, 271 (1973).
[23] C.D. Carpentier and R. Nietsche, Mater. Res. Bull. **9**, 1097 (1974).
[24] G. Dittmar and H. Schäfer, Z. Naturforsch. B **29B**, 312 (1974).
[25] B. Scott, M. Pressprich, R.D. Willit, and D.A. Cleary, J. Solid State Chem. **96**, 294 (1992).
[26] A. Ruediger, O. Schirmer, S. Odoulov, A. Shumelyuk, and A. Grabar, Opt. Mater. **18**, 123 (2001).
[27] R. Caracas and X. Gonze, Phys. Rev. B **66**, 104106 (2002).
[28] V. Fenchak, I. Kityk, A. Grabar, and V. Slivka, Ferroelectrics **192**, 129 (1997).
[29] G.M. Currò, V. Grasso, F. Neri, and L. Silipigni, Nuovo Cimento D **20**, 1163 (1998).
[30] A.N. Gusatinskii, A.A. Lavrentev, M.A. Blokhin, and V.Y. Slivka, Phys. Status Solidi B **131**, 139 (1985).
[31] Y. Ohno and K. Hirama, J. Solid State Chem. **63**, 258 (1986).
[32] P. Blaha, K. Schwarz, and J. Luitz, computer code WIEN97

(Vienna University of Technology, Vienna, 1997); improved and updated version of original copyrighted WIEN code: P. Blaha, K. Schwarz, P. Sorantin, and S.B. Trickey, Comput. Phys. Commun. **59**, 399 (1990).

[33] J. Chastain, *Handbook of X-Ray Photoelectron Spectroscopy* (Perkin Elmer, Eden Prairie, 1992).

[34] J.J. Jia *et al.*, Rev. Sci. Instrum. **66**, 1394 (1995).

[35] J. Perdew and Y. Wang, Phys. Rev. B **45**, 13 244 (1992).

[36] D. Singh, Phys. Rev. B **43**, 6388 (1990).

[37] P. Blöchl, O. Jepsen, and O. Andersen, Phys. Rev. B **49**, 16 223 (1993).

[38] S. Tougaard, J. Electron Spectrosc. Relat. Phenom. **52**, 243 (1990).

[39] M. M. Maior, Phys. Solid State **41**, 1333 (1999).

[40] D. Baltrunas, A. Grabar, K. Mazeika, and Y. Vysochanskii, J. Phys.: Condens. Matter **11**, 2983 (1999).

[41] The interstitial part brings a large contribution to the TDOS, due to the openness of the structure. This contribution exhibits all features discussed with respect to individual PDOS, and it is difficult to decompose it for a more detailed anlysis. The TDOS per unit cell in Fig. 3 includes the interstitial contribution.